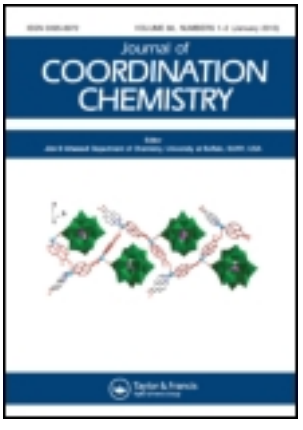

Journal of Coordination Chemistry
Publication details, including instructions for authors and subscription information:
http://www.tandfonline.com/loi/gcoo20

Solution and solid-state spectroscopic characterization of chloro dimethylsulfoxide polythioether ruthenium(II) complexes, complemented with DFT calculations in the gas phase

João Madureira [a b] & Teresa M. Santos [a]

[a] Departamento de Química e CICECO , Universidade de Aveiro , Aveiro , Portugal

[b] Department of Chemistry , Virginia Commonwealth University , Richmond , VA , USA

Accepted author version posted online: 29 Jan 2013.Published online: 15 Mar 2013.

To cite this article: João Madureira & Teresa M. Santos (2013) Solution and solid-state spectroscopic characterization of chloro dimethylsulfoxide polythioether ruthenium(II) complexes, complemented with DFT calculations in the gas phase, Journal of Coordination Chemistry, 66:5, 881-903, DOI: 10.1080/00958972.2013.770846

To link to this article: http://dx.doi.org/10.1080/00958972.2013.770846

Journal of Coordination Chemistry
Vol. 66, No. 5, 10 March 2013, 881–903

Solution and solid-state spectroscopic characterization of chloro dimethylsulfoxide polythioether ruthenium(II) complexes, complemented with DFT calculations in the gas phase

JOÃO MADUREIRA†‡* and TERESA M. SANTOS†

†Departamento de Química e CICECO, Universidade de Aveiro, Aveiro, Portugal;
‡Department of Chemistry, Virginia Commonwealth University, Richmond, VA, USA

(*Received 2 August 2012; in final form 29 November 2012*)

Several ruthenium(II)-chloro-dimethylsulfoxide complexes with formulae $[RuCl_2(DMSO)(k^3\text{-}L_1)]$ or $[RuCl(DMSO)(k^4\text{-}L_2)]^+$, where $L_1 = [9]aneS_3$ (**2**) or ttbt (**5**) and $L_2 = [12]aneS_4$ (**3**), $[14]aneS_4$ (**4**) or $[14]aneN_4$ (**6**), have been synthesized from *cis*,*fac*-$[RuCl_2(S\text{-}DMSO)_3(O\text{-}DMSO)]$ (**1**) and the respective macrocycle. They were spectroscopically characterized by FT-IR, FT-Raman, NMR, and UV/Vis. Particular attention was given to *fac*-$[RuCl_2(DMSO)(k^3\text{-ttbt})]$ (**5**), the first octahedral complex of ttbt, which was also studied by DFT calculations. The behavior of the complexes in coordinating solvents water, acetonitrile, and dimethylsulfoxide was studied to understand their reactivity and predict the resulting ions formed in solution. The role of the counter ion (Cl^- *vs*. PF_6^-) was also evaluated. The results indicate that the chosen macrocycle, the counter-ion, and the solvent have a direct impact on the chemical species formed in solution.

keywords: Ruthenium; Crown thioethers; Counter-ion; Solvolysis; Molecular modeling

1. Introduction

Complexes with macrocyclic ligands represent classic coordination chemistry. Among them, crown thioethers became increasingly popular, starting in the late 1980s [1–6]. They are more commonly used as ligands with second and third transition elements series, but several complexes of the first series of transition elements were already produced [1,7,8]. They stabilize metal centers with high electron density, even for uncommon and typically unstable oxidation states like Ag(II), Au(II), Rh(II), or Pd(III) [2,9].

One, 1,4,7-trithiacyclononane ([9]aneS$_3$), became the object of many studies in coordination chemistry because of its unique properties among polythioethers, with its lower energy conformations fully or partially endodentate [10,11]. The very high chemical robustness of [9]aneS$_3$ complexes also permitted imaging compounds (^{99m}Tc) [12] or γ-emitting isotopes (^{186,188}Re) [13] to be developed and explored in nuclear medicine. Recently, Ru(II) and Rh(III) complexes with [9]aneS$_3$ have also been tested as anti-tumor candidates [14].

*Corresponding author. Email: jlmadureira@vcu.edu

ISSN 0095-8972 print/ISSN 1029-0389 online
http://dx.doi.org/10.1080/00958972.2013.770846

Besides [9]aneS$_3$, other macrocycles used in coordination compounds presented in this study include 1,4,7,10-tetrathiacyclododecane ([12]aneS$_4$), 1,4,8,11-tetrathiacyclotetradecane ([14]aneS$_4$), 3,6,9,14-tetrathia-bicyclo[9.2.1]tetradeca-1(13),11-diene (ttbt), and 1,4,8,11-tetraazacyclotetradecane ([14]aneN$_4$) (scheme 1). With the exception of ttbt, coordination chemistry of these crown thioethers has been extensively studied [15–18]. Ttbt has only been used for a few coordination compounds, with Cu(II), Ag(I), Pd(II) and Pt (II), [16,19–22]. Furthermore, while many of the more common crown thioethers have been studied by theoretical means [11,23,24], this is not the case with ttbt or its complexes. We here present some of our DFT results with ttbt and its first ruthenium and octahedral complex, [RuCl$_2$(DMSO)(k^3-ttbt)] and compare them with the available X-ray data [25].

Ruthenium–halo–sulfoxide complexes have been studied during the last decades in the area of medicinal chemistry, mainly for anticancer activity [25,26]. Sulfoxides increase both lipophilic and hydrophilic properties of metal drugs, resulting in less toxic derivatives, compared with their parent chloro-complexes, while keeping their chemotherapeutic activity [27].

Only a few ruthenium polythioether complexes with DMSO and chloro ligands are known [15,28–31]. These compounds are of interest as adequate precursors for polypyridyl–polythioether complexes, but also in themselves, since they might have interesting properties that result from the combination of the increased stability imposed by crown thioethers and the lipophilicity and aqueous solubility of DMSO–ruthenium complexes [30,32,33].

In this article, we present some of our work on chloro dimethylsulfoxide polythioether ruthenium(II) complexes, some previously published and other new, that belong to a class of compounds that has been barely studied. Besides the spectroscopic characterization

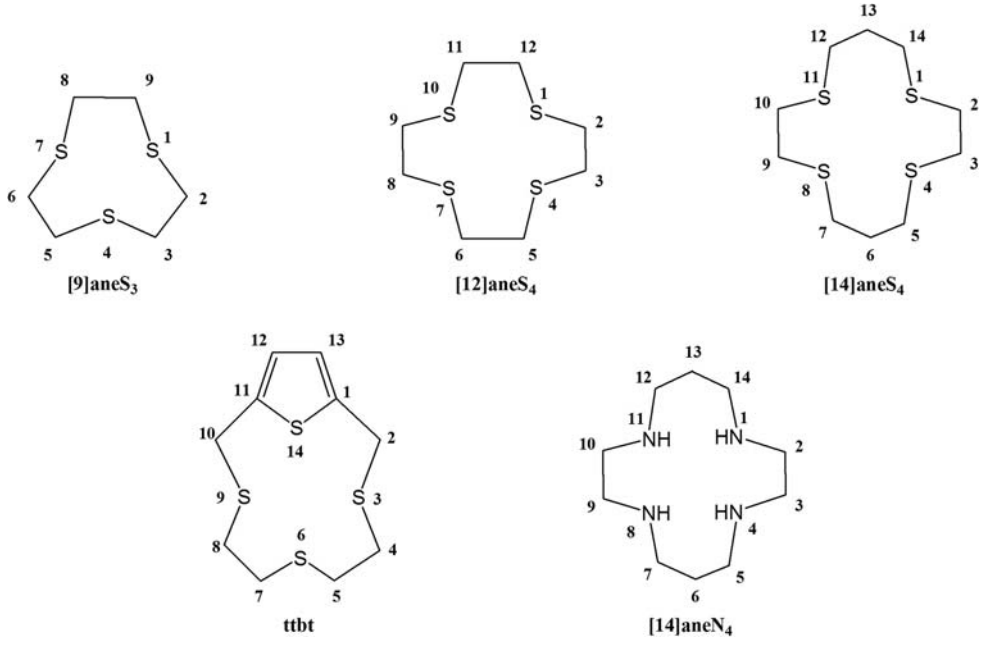

Scheme 1. Macrocycles studied in this work.

(UV/Vis, FTIR, Raman and NMR), we also include reactivity tests of the compounds in aqueous and organic media with coordination ability (CH_3CN, DMSO) and perform an analysis of the counter ion role (Cl^- *vs*. PF_6^-). Wherever necessary, the deuterated DMSO derivatives, same as their bromo and iodo analogs, have been synthesized and characterized to ensure unambiguous assignments in the solid state.

2. Results and discussion

2.1. *Synthesis of complexes*

Six of the seven complexes discussed in this article are indicated in scheme 2, along with their preparation methodology; the proposed structures are consistent with NMR, FT-IR, and EA or ESI-MS characterization. Compounds **1–4** were prepared with small variations from the literature procedures [15,28,30,34]. The deuterated derivative of **1**, *cis*-[$RuCl_2$(DMSO-d_6)$_4$], **1a**, was used in the synthesis of *fac*-[$RuCl_2$(DMSO-d_6)([9]aneS$_3$)], **2a**, and *cis*-[RuCl(DMSO-d_6)([12]aneS$_4$)]Cl, **3a**, combining it with the respective macrocycles. Compounds *fac*-[$RuBr_2$(DMSO)([9]aneS$_3$)], **2b**, and *fac*-[RuI_2(DMSO)([9]aneS$_3$)], **2c**, were obtained by solubilizing **2** in water in the presence of an excess of NaBr or CsI, respectively.

While **1–4** were prepared in good yields, the synthesis of [$RuCl_2$(DMSO)(k^3-ttbt)], **5**, where ttbt is 3,6,9,14-tetrathia-bicyclo[9.2.1]tetradeca-1(13),11-diene (scheme 1), gave a lower yield (25%) and required a purification step comprising an extraction in chloroform. The hypothetically tetradentate, complex **5**, shows ttbt in a tri-coordinated form. Such a coordination mode can be explained by the stiffness imposed by the thiophene ring in the macrocyclic skeleton [21,22,35]. The formula assigned to **5** is consistent with solid state (FT-IR and EA) and solution (NMR) data [36]. Both NMR and infrared data confirm sulfur coordination of DMSO. The neutral charge formula is also consistent with the very low observed solubility of the formed complex in almost all common organic solvents. Theoretical calculations at the DFT level (see Sections 2.5 and 3.2) indicate a preference for *fac* coordination that was recently confirmed by a single crystal X-ray structure [25,37].

Although ttbt has been known for almost 25 years [20], a detailed literature survey indicates that **5** is the only known coordination compound with octahedral geometry. In fact, **5** was only presented in the PhD thesis of this study's first author and has been made recently available electronically [37] in the PhD thesis of Dr E.L.S. Cheu [25].

We also used the polyamine analog of [14]aneS$_4$ to prepare [RuCl(DMSO)([14]aneN$_4$)]PF_6, **6**, which was isolated as a light yellow solid with a yield of 44%. Ru(II) complexes with un-oxidized polyamines are not so common [38], since they tend to oxidize to their polyimine analogs. The synthesis of **6** presents the reproducibility problems already seen in other ruthenium reactions with [14]aneN$_4$ [39–43]. A gradual darkening and color change to green can be seen after some weeks even in the solid state. Since NMR indicates that a diamagnetic complex is still in solution, it seems plausible that oxidative dehydrogenation of the polyamine catalyzed by the coordination metal ion occurs. This is a common phenomenon with aliphatic polyamines, particularly when coordinated to group VIII metal ions [40,43]. Probably the presence of DMSO in the coordination sphere slows down the reaction, due to its stabilization of Ru(II).

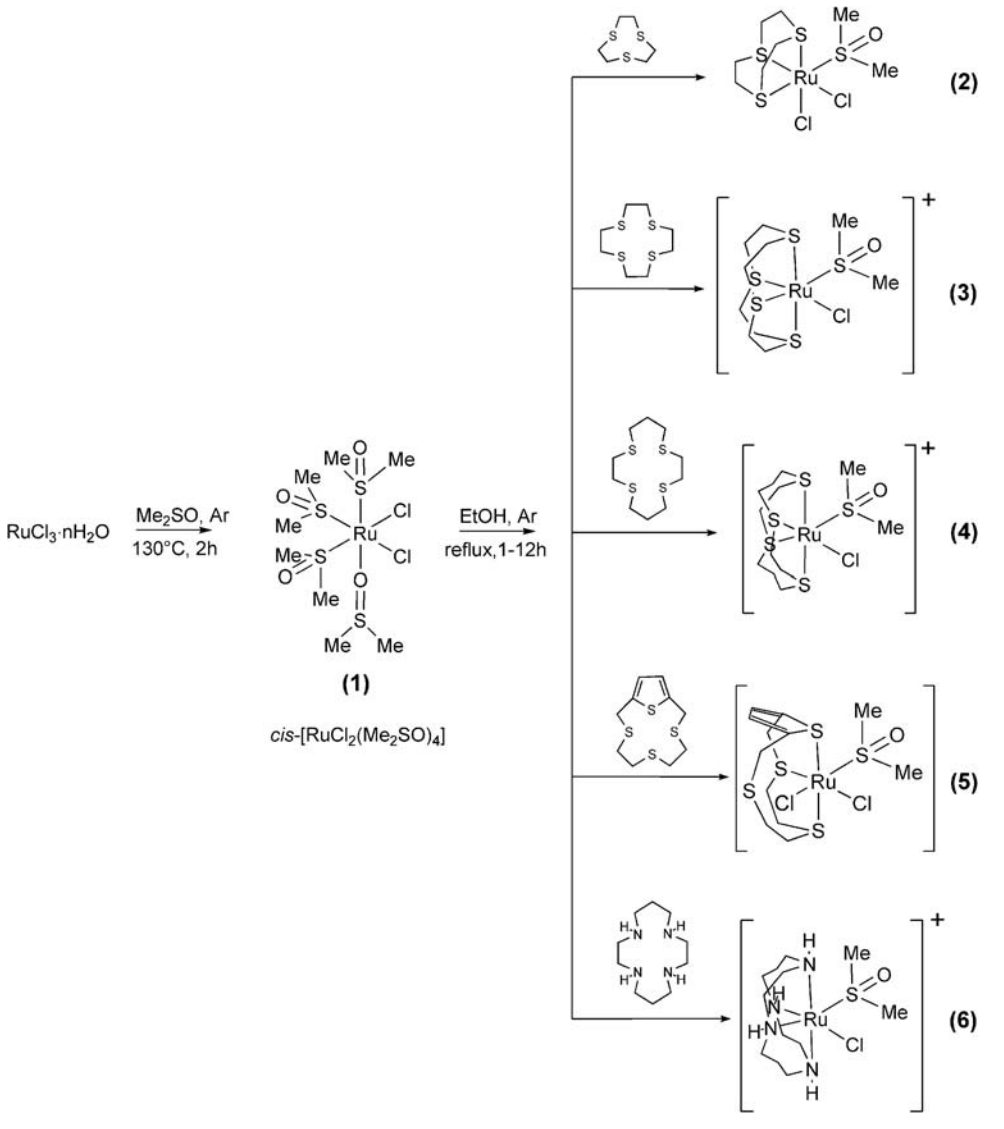

Scheme 2. Synthesis of **1**–**6**.

Finally, $[RuCl(CH_3CN)(DMSO)([9]aneS_3)]PF_6$, **7**, was prepared from **2** and NH_4PF_6 in CH_3CN (see Sections 2.6 and 3.3), which is a relatively rare example of a {M([9]aneS$_3$)} octahedral complex with different monodentate ligands on all the remaining coordination positions [44,45].

Complex **1** is prepared in pure DMSO. Because of its high viscosity, the solvent tends to remain attached to the compound even after washing with different solvents and a variable amount of free DMSO is always present in the precursor and the remaining complexes. To minimize the DMSO excess and the possibility that $[RuCl(DMSO)_2([9]aneS_3)]^+$ competes with $[RuCl_2(DMSO)([9]aneS_3)]$, **2**, during its preparation, the complex was recrystallized in ethanol.

In **2–7**, only *S*-DMSO coordination is observed. This is the most common coordination mode in Ru(II) compounds, as shown by structural data and theoretical calculations [46–48]. Such a preference results from the high electronic density of Ru(II), adequate orbitals for π bonding and absence of, or just moderate, *trans* π-acceptor competition (chloride acts as a π-donor, while thioethers are also π-acceptors, although considerably weaker than DMSO) [28–30,49].

2.2. *Infrared absorption and Raman diffusion spectroscopy*

Assignment of the coordination sphere vibration modes in ruthenium(II) complexes, like in any other metal ion with small force constants, is normally not made without some degree of uncertainty. Stretching and bending modes related with the metal ion and the binding positions occur on the lower energy detection limit of many infrared devices. At such frequencies, there is also loss of transparency of common materials for pellet preparation (CsI and, particularly, KBr). Furthermore, assignments become complicated because metal-ligand and ligand vibration modes typically overlap, the same as combination modes or crystal packing associated bands.

In order to help the assignments, deuterated homologues of **1–3** and halogenated derivatives of **2** were prepared. Their infrared and Raman spectra were compared with their equivalents of $[Ru([9]aneS_3)_2](PF_6)_2$, $[RuCl(CH_3CN)([12]aneS_4)]PF_6$, and $[Ru(CH_3CN)_2([12]aneS_4)](PF_6)_2$, the same as for their respective macrocycles.

All complexes show vibrational bands at wave numbers that are typical of Ru–S (DMSO) and Ru–halogen bond stretches. Compounds **2–5** and **7** also show bands assigned to Ru–S stretching modes from the crown thioethers (table 1).

Based on the observed shifts of the characteristic sulfoxide stretching, it was also possible to differentiate between sulfur-bonded and oxygen-bonded DMSO, since linkage isomers show different frequency ranges.

Combined use of absorption (IR) and diffusion (Raman) vibrational techniques allow methyl ν_{C-H} and $\nu_{S=O}$ stretching modes in DMSO to be distinguished from the methylene ν_{C-H} and δ_{C-H} modes in the macrocycles, respectively.

2.2.1. Metal-ligand stretching and bending mode. The *fac*-$[MS_3X_2Y]$ complexes with a pseudo-octahedral environment around the central M belong to the C_s point group with three ν_{M-S}, two ν_{M-X} and one ν_{M-Y} stretching modes, active in both the infrared and Raman spectra. The compounds *cis*-$[MN_4/S_4XY]$ also belong to the C_s point group and present four $\nu_{M-N/S}$ vibrations, one ν_{M-X} and one ν_{M-Y}, all infrared and Raman active [50]. In polyamine or polythioether macrocycle complexes several conformations might coexist at r.t., with the macrocycle imposing distortions to the pseudo-octahedral geometries, resulting in an increment in the number of bands.

Assignments of the vibrational bands at 500–200 cm^{-1} for **1–7** are presented in table 1. A more detailed analysis was performed for **1–3** based on the comparison with their DMSO-d_6 analogs (**1a**, **2a**, **3a**), and the bromo (**2b**) and iodo (**2c**) forms of **2** (see Section 3.3 and tables S1–S3 in Supplementary material).

Stretching bands for Ru–S (DMSO) and Ru–S (thioether) show similar intensity in the Raman spectra, but the first type is much more intense in the infrared (figure 1). The Ru–S (DMSO) stretch is seen at 420–430 cm^{-1}, sometimes with a less intense one near

Table 1. Infrared and Raman vibrational mode assignment (500–200 cm^{-1}) for **1–7**.

	$\nu_{Ru-Smacro}$		ν_{Ru-S} (DMSO)		ν_{Ru-O} (DMSO)		δ_{C-S-O}		ν_{Ru-N}		ν_{Ru-Cl}	
Complexes	IR	R	IR	R	IR	R	IR	R	IR	R	IR	R
$[RuCl_2(DMSO)_3(DMSO)]$, **1**			448	448	483	476	389	384			264*sh*	255
			425	424							246*b*	
$[RuCl_2(DMSO)([9]aneS_3)]$, **2**	493	493	456				377	377			274*d*	276
	456	458	421	421							261	263
$[RuCl(DMSO)([12]aneS_4)]Cl$, **3**	460*s*	455	422	421			377	380*d*			271	272
	447*h*	448										
	436	439										
$[RuCl(DMSO)([14]aneS_4)]PF_6$, **4**	466		428				379				273	
	439											
$[RuCl_2(DMSO)(k^3\text{-ttbt})]$, **5**	488[a]	488	430	432			378	380				277
	468*sh*	468										264*b*
$[RuCl(DMSO)([14]aneN_4)]PF_6$, **6**			442	444			379	397		253	280	282
			424*sh*							239		
$[RuCl(MeCN)(DMSO)([9]aneS_3)]PF_6$, **7**	493	496	430	428			377	377		224	247	248
	460*b*	461										
$[Ru(MeCN)_3([9]aneS_3)](PF_6)_2$	496	495								200		
	467*d*	466*d*										
	425*b*	432										
	412[b]	412[b]										
$[Ru([9]anoS_3)_2](PF_6)_2$	495											
	471	471										
	461	458										
		430										

[a]Eventually from *ttbt* (491 cm^{-1}).
[b]Probably ν_5 of PF_6^-, observed in TBA-PF_6 and $TlPF_6$ Raman spectra at 418 and 414 cm^{-1}, respectively.
Notes: *b* – broad; *d* – doublet; and *sh* – shoulder.

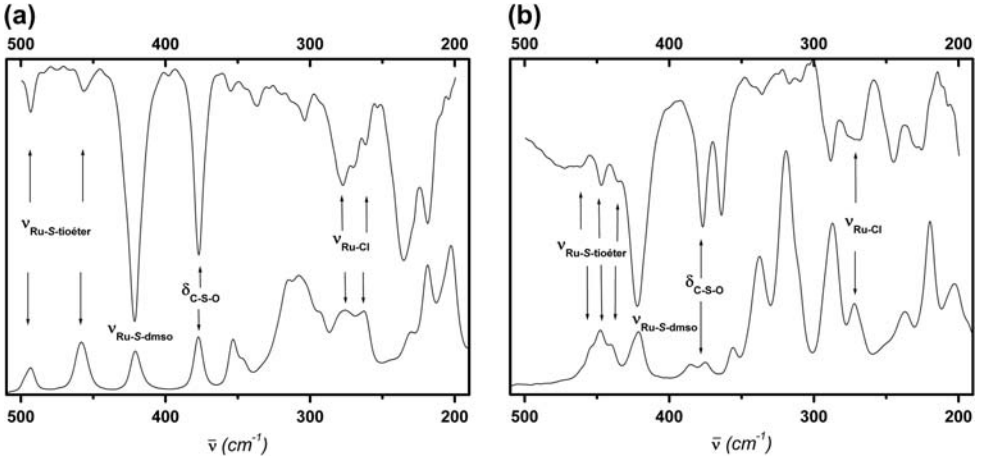

Figure 1. Infrared (top) and Raman spectra (bottom) of the vibration modes on the 500–200 cm^{-1} range for (a) *fac*-$[RuCl_2(DMSO)([9]aneS_3)]$, **2** and (b) *cis*-$[RuCl(DMSO)([12]aneS_4)]Cl$, **3**.

450 cm^{-1}. Ru–S (thioether) stretching occurs between 420 and 490 cm^{-1} with two to four bands.

Complexes **1–5** and **7** present ν_{Ru-Cl} bands between 246 and 277 cm^{-1}, while [RuCl(DMSO)([14]aneN$_4$)]PF_6, **6**, shows two weak bands at 258 and 280 cm^{-1}, in the infrared, and two at 266 and 282 cm^{-1}, in the Raman spectra. Previously published literature data on Ru–Cl stretches covers the range 240–275 cm^{-1} [39,51,52]. X-ray data show that Ru–Cl bonds where Cl is *trans* to polythioethers or DMSO are significantly longer than expected for a pure σ donor [53], indicating π back donation. A slight increase in the Ru–Cl wavenumber is expected for **6**, since no π back donation is present with the amine macrocycle.

Ru–N stretching modes are expected below 250 cm^{-1} and only a few of such vibration modes are found in the literature. Because of this, the values of ν_{Ru-N} presented in table 1 for **6** and **7** should be considered as tentative assignments.

2.2.2. Other characteristic vibration modes. The S=O stretching is the most characteristic vibration mode of DMSO. As free solvent, it appears at 1055 cm^{-1}. Metal coordination through S increases the double bond character of sulfoxide, shifting the band to higher wave numbers. When metal binding occurs as *O*-DMSO, the band moves to lower energy, since the zwitterionic form is favored (single bond). Since all complexes show a strong band or a doublet near 1100 cm^{-1} [46], an *S*-DMSO coordination mode is assigned: **2** (1088 cm^{-1}), **3** (1092 and 1077 cm^{-1}), **4** (1084 cm^{-1}), **5** (1088 cm^{-1}), **6** (1081 cm^{-1}) and **7** (1100 and 1092 cm^{-1}) [54]. Complex **1**, with a crystal structure that establishes the presence of three coordinated *S*-DMSO and one *O*-DMSO, shows vibrations in both regions: 1107 and 1086 cm^{-1} (*S*-DMSO) and 925 cm^{-1} (*O*-DMSO) [53]. Another characteristic vibration of DMSO is δ_{C-S-O}, seen for **1–7** at 377–389 cm^{-1}.

Acetonitrile coordination to the metal ion is signaled in the infrared and Raman spectra of **7** by two weak to medium intensity bands at 2314 and 2286 cm^{-1}, being more intense in the Raman. The observed values agree well with data for ruthenium(II)–acetonitrile–polythioethers complexes [15,28,30].

2.3. *Nuclear magnetic resonance spectroscopy*

^{1}H NMR spectra of the compounds present an aliphatic region with a series of multiplets that correspond to macrocycle methylene groups and sharp singlets from methyl protons of DMSO (**1–7**) and CH_3CN (**7**). All prepared complexes show singlets between 3.0 and 3.5 ppm, in different solvents, assigned to S-coordination of DMSO. This one is characterized by a deviation to weak field of approximately 1 ppm by comparison with the solvent (2.55 ppm in DMSO-d$_6$), while the O-coordination mode causes only a slight shift to weak field (*ca.* 0.1 ppm) [55]. Two slightly different environments, separated by 0.02 to 0.07 ppm, and equally intense can be seen in the complexes. Since it is highly improbable that all macrocycles show two macrocycle conformations in equilibrium with the same 1 : 1 relative abundance at r.t., they probably result from alternative environments of each methyl in DMSO. While the vibrations of DMSO with a major rotation component around Ru–S or C–S (methyl rotation) are typically free at r.t., they correspond to small displacements from their equilibrium positions and not full rotation around the bond axis. For that,

much more energy is required to surpass the energy barriers that result from loss of stabilizing interactions between DMSO and other parts of the molecule, and possible repulsion that occurs for certain rotation angles. Another piece of information that supports this interpretation is the fact that **3** shows two environments in CH_3CN, but only one in D_2O. Since there are no signs of exchange of DMSO by CH_3CN or water, the differences observed among the solvents might come from their different ability to establish interactions with coordinated DMSO that, in the case of water, might override the internal interactions that exist in the complex.

Complex **2** also presents a single DMSO environment in CD_3NO_2 (figure S1), in contrast to other complexes that show two environments in this solvent. Nevertheless, in the solid state the CP-MAS and HP Dec-MAS NMR spectra show two methyl environments at 42.3 ppm ($J = 83$ Hz) and 46.9 ppm ($J = 68$ Hz), as seen in figure 2, as a result of structure rigidification caused by packing. The values appear in a range similar to other Ru(II)–*S*-DMSO complexes [55]. While ^{13}C CP-MAS shows only two environments for free [9]aneS_3, at 21.5 and 27.2 ppm, coordination causes loss of symmetry and shifts the chemical environments to weak field, with a series of multiplets between 26 and 41 ppm assigned to CH_2–S [30,56]. It was not possible to solve these environments in the HP Dec-MAS spectrum of **2**, even with a relaxation time of up to 120 s, acquisition time of up to 48 h, and proton decoupling in the power limit range. Such behavior comes from different relaxation times of the different environments, which will be emphasized if two alternative conformations of [9]aneS_3 coexist at r.t. in the solid state. Nine different ^{13}C environments for [9]aneS_3 suggest two conformers: a more symmetric one with C_s symmetry (three environments) and a C_1 form, where all six carbons are magnetically different.

Complex **5**, [$RuCl_2$(DMSO)(k^3-ttbt)], is almost insoluble in common organic solvents. In DMSO, where it is moderately soluble, a fast ligand exchange can be seen. The ^1H NMR was acquired in $CDCl_3$ but due to the very low solubility, it was more difficult to analyze and prevented the acquisition of a NOESY spectrum. The aliphatic region of the complex shows a large number of doublets (figure 3). Besides a major set of peaks, weaker ones are also clearly seen (*ca.* 1 : 5). Since purity of the compound has been established for several samples and further purification did not change the spectrum, it seems that several forms of the complex coexist. Two equally intense signals at 7.12 ppm and 7.06 ppm assigned to the thiophene protons could be seen, in contrast to the free macrocy-

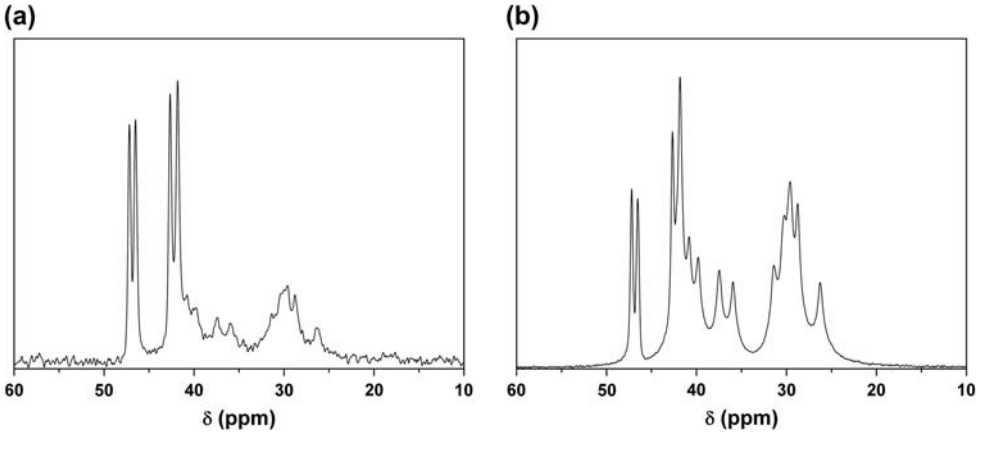

Figure 2. ^{13}C MAS spectra of *fac*-[$RuCl_2$(DMSO)([9]aneS_3)], **2**. (a) HP Dec-MAS. (b) CP-MAS.

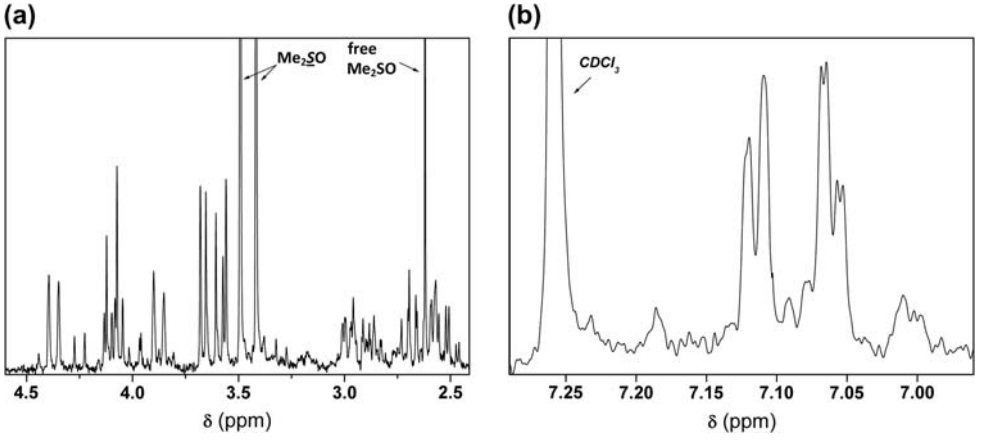

Figure 3. ^{1}H NMR of *mer*-[RuCl$_2$(DMSO)(k^3-ttbt)], **5**, in CDCl$_3$. (a) Left – aliphatic protons of ttbt and DMSO. (b) Right – aromatic protons of the thiophene component.

cle that shows a single environment at 6.92 ppm, as a result of fast exchange between ttbt conformers. In DMSO-d$_6$, two new environments with the same intensity are seen at 7.18 and 6.98 ppm, assigned to the thiophene unit protons. Furthermore, there is an increase in free DMSO environments.

The highest known coordination number of ttbt macrocycle is three, despite its four available coordination positions. In **5**, the two environments for the thiophene unit and the large number of methylene environments, for both major and minor sets of signals, support an asymmetrically coordinated crown thioether that is rigid at r.t.

While Pd(II)/Pt(II)–ttbt complexes are flexible enough to permit conformer interconversion or fluxion between available positions for coordination in k^3 systems [21,22], a typical octahedral coordination metal ion, like Ru(II), results in more rigid crown thioether coordination structures, because the energy barriers between ttbt conformers are expected to increase.

The more probable explanation for the ^{1}H NMR of **5** in CDCl$_3$ is an asymmetrically coordinated ttbt with more than one geometric isomer or conformer. To clarify this situation, theoretical calculations were performed for **5**, which are presented and discussed in Sections 2.5 and 3.2.

The spectrum of [RuCl(DMSO)([14]aneN$_4$)]PF$_6$, **6**, in CD$_3$NO$_2$ confirms the diamagnetic nature of the complex. Besides the usual macrocycle and DMSO environments, four weak environments can be seen between 8.0 and 8.6 ppm, assigned to amine protons. Since the large majority of {Ru([14]aneN$_4$)} complexes with monodentate ligands are Ru(III), such stabilization of Ru(II) must come from the coordinated *S*-DMSO.

[RuCl(CH$_3$CN)(DMSO)([9]aneS$_3$)]PF$_6$, **7**, shows besides the polythioether and DMSO environments, a singlet near 2.7 ppm (in acetone-d$_6$), assigned to coordinated acetonitrile (figure S2).

2.4. *UV/Vis spectroscopy*

Complexes **1–7** show absorption bands in the visible region of the spectrum with maxima between 370 and 420 nm and colored solutions from a pale yellow to deep orange. The upper limit is observed in complexes with the higher number of coordinated chloro groups.

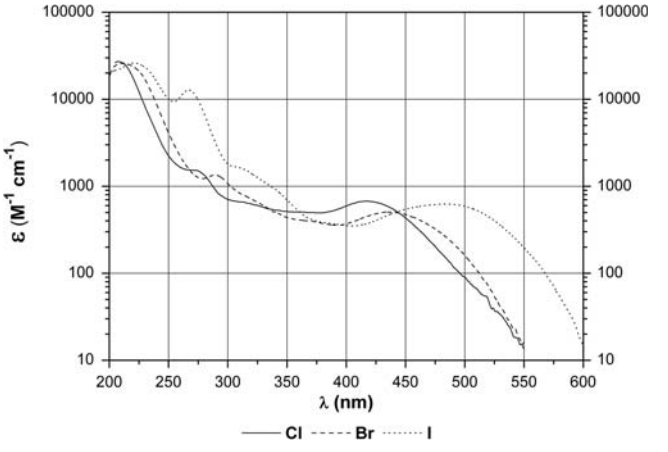

Figure 4. UV/Vis spectra of [RuX_2(DMSO)([9]aneS_3)] (X = Cl, Br, I) in ethanol at 20°C. (—) chloro, (- - - -), bromo, (…) iodo.

The absorptions in the visible region have molar absorptivity coefficients below 10^3 M^{-1} cm^{-1}. To help the assignments, the chloro, bromo, and iodo forms of **2** were prepared and their UV/Vis spectra are represented in figure 4.

The electronic spectra of low-spin octahedral d^6 complexes are expected to present two spin allowed transitions at relatively low energy: $^1A_{1g} \rightarrow {}^1T_{1g}$ and $^1A_{1g} \rightarrow {}^1T_{2g}$. The complexes *cis*,*fac*-[RuX_2(*S*-Me_2SO)([9]aneS_3)] present a much lower symmetry (actually C_1). Ignoring the chelate rings of [9]aneS_3, it can be approximated to C_s. If we also consider that the polythioether and dimethylsulfoxide electronic impact is not so different, it can be further approximated to *cis*-[$RuX_2(S)_4$], with C_{2v} punctual symmetry. These approximations are expected to hold well for the electronic spectra interpretation since the *effective* symmetry depends mainly on the type of ligand atoms bonded to the metal center. The T_{1g} and T_{2g} terms in O_h are split in A and B terms, and six transitions are predicted instead of two. Despite this, only three bands are commonly seen since several show reduced splitting: v_1 (B_1 from T_{1g}), v_2 (A_2 and B_2 from T_{1g}), and v_3 (A_1, A_2 and B_2 from T_{1g}). More intense charge transfer bands overlapping the d–d bands are also common. They can be either MLCT or LMCT types (to orbitals centered on the S atoms and from LUMO orbitals of the halogens, respectively).

The electronic spectra of **2**, **2b,** and **2c** were convoluted with multi-Gaussians in order to determine all transitions that might be overlapped (figures S5–S7). The compounds have five regions in common with maxima at 417–480 nm ($\varepsilon \approx 5.0$–6.7×10^2 M^{-1} cm^{-1}), 352–359 nm ($\varepsilon \approx 1.6$–3.8×10^2 M^{-1} cm^{-1}), 308–334 nm ($\varepsilon \approx 3.5$–6.3×10^2 M^{-1} cm^{-1}), 276–307 nm ($\varepsilon \approx 7.0$–12.4×10^2 M^{-1} cm^{-1}), and a last more intense band (*ca.* 3×10^4 M^{-1} cm^{-1}) at 208–221 nm. The first two absorptions of the spectrum (λ in nm, ε in 10^{-3} M^{-1} cm^{-1}) of the related complex *cis*-[RuX_2([14]aneS_4)] appear at 430–455 (0.12–0.18) and 363–380 (0.90–1.02) [51].

The lowest energy bands are too intense to be classified as spin-forbidden transitions. Except for the higher energy band, they are plausibly d–d transitions, in line with their modest intensity and the wavelength evolution that follows the spectrochemical series. In fact, increasing the π-donor strength, according to the order chloro < bromo < iodo, should cause a gradual increase in the energy of Ru(II)-filled d orbitals and a decrease in the

ligand-field splitting parameter, moving transitions to red, as is typically seen in more regular octahedral systems (t_{2g} to e_g energy gap).

The higher energy band is assigned to a MLCT transition where the acceptor orbital is probably σ^*_{C-S}, as seen in other Ru(II)–[9]aneS$_3$ complexes [57,58].

Besides these bands, complex **2c** shows an extra one at 267 nm, which might have its origin in a double excitation of d–d type, as is known to occur in other iodo complexes [40,42,43].

Ligands *trans* to one another interact with the same *d* orbital and the combined impact of the two ligands can be approximated to the average of the impact of each one. For the complexes under study, the axial field strength is then caused by two sulfurs, while in the equatorial plane, it corresponds to the average of S and X field strength. Such interpretation permits to treat the *cis* series as a trigonal distortion to O_h, like seen for the series *trans*-[RuX$_2$(S)$_4$]. Such distortion causes the splitting of the $^1A_{1g} \rightarrow {}^1T_{1g}$ band in $^1A_{1g} \rightarrow {}^1E_g$ and $^1A_{1g} \rightarrow {}^1A_2$. The splitting of $^1T_2$ is usually neglected, and a single transition corresponding to $^1A_{1g} \rightarrow {}^1T_{2g}$ is expected. Higher energy bands should have charge transfer nature.

As an example, the related *trans*-[RuX$_2$(S)$_4$], where S$_4$ = (Me-S-S-Me)$_2$ and X = Cl or Br, the three bands are detected *ca.* 21,000 cm^{-1}, 29,000 cm^{-1}, and above 30,000 cm^{-1} [59]. Assuming the average impact of the ligands force field *trans* to each other, the first two transitions in the *cis* analog are predicted to occur near 25,000 and 29,000 cm^{-1}, respectively, which is similar to our experimental results.

The trigonal model predicts four electronic transitions but has five parameters – Dq, Dt, Ds, B, and C – where Dq is the octahedral crystal field parameter, Dt and Ds are the tetragonal field parameters, and B and C are the relevant Racah parameters. Dt is a measure of the difference between the Dq values of equatorial and axial ligands (for details on the model see the literature) [60]. To solve such equations it is common to consider $C \approx 4 \cdot B$ and neglect the splitting of the $^1T_{2g}$ term giving an average energy for ν_3 and ν_4. Since **2**, **2b,** and **2c** have four transitions less intense than 1000 M^{-1} cm^{-1}, but the last one occurs at wavelengths below 300 nm, it is questionable that all four correspond to d-d transitions and calculations were performed for the two hypotheses.

The equation systems were solved with Derive™ v.6.1 from Texas Instruments for the wavelengths determined with the multi-Gaussian fitting (Origin® v.7.1). It was considered that the order of $^1A_{1g} \rightarrow {}^1E_g$ and $^1A_{1g} \rightarrow {}^1A_2$ transitions is inverted by comparison with the *trans* series.

Table 2. Characterization of the electronic spectra of [RuX$_2$(DMSO)([9]aneS$_3$)] (X = Cl, Br, I): maxima and absorptivity obtained by multi-Gaussian fitting, crystal field and Racah parameters (all values in cm^{-1}, except ε in 10^{-3} M^{-1} cm^{-1}).

	λ [ε]	Dq	Ds	Dt	B	C
cis-[RuCl$_2$(DMSO)([9]aneS$_3$)], **2**	24,008 [0.65]	2609	539	−461	520	2079
	28,039 [0.16]					
	32,471 [0.63]					
	36,282 [0.70]					
cis-[RuBr$_2$(DMSO)([9]aneS$_3$)], **2b**	22,878 [0.50]	2456	476	−631	421	1685
	28,398 [0.35]					
	30,867 [0.35]					
	34,514 [1.21]					
cis-[RuI$_2$(DMSO)([9]aneS$_3$)], **2c**	20,830 [0.67]	2237	263	−807	385	1540
	27,887 [0.38]					
	29,968 [0.58]					
	32,557 [1.24]					

While both hypotheses give small differences on Dq values (400–600 cm^{-1}) and the right decrease in Dq: Cl > Br > I, only when considering the splitting of the third and fourth transition, values obtained for the main Racah parameter, B, follow the expected steady decrease in magnitude, with Cl > Br > I (table 2). Concomitantly, the magnitude of Dt augments, indicating the increase in the difference on the field strength between sulfur and the halogen.

2.5. *Molecular modeling*

Previous studies on complexes with different macrocycles have shown that DFT can adequately modulate their structural, energetic, and conformational preferences [17,61], but so far only a few crown thioether transition metal complexes have been studied by theoretical methods [17,24,58,62]. Here, theoretical calculations at the DFT level were performed for ttbt and *fac*-[$RuCl_2$(DMSO)(ttbt)], **5**, that have their geometries established in the crystalline solid state. Calculations for ttbt were performed first to assess the ability of different models to mimic its experimental X-ray crystal structure (table S4) [20]. Calculated and experimental structures are in good agreement as can be seen in figure S3 for calculations at the B3LYP/6-311+G(2d,p) level (RMSD = 0.09 Å, heavy atoms only). The minimized structure correctly predicts that all sulfurs are exocyclic and almost in the same plane, with the thiophene unit almost perpendicular to it, as seen in the X-ray crystal structure.

Calculations for **5** were performed at the B3LYP/6-311+G(2d,p)/LANL08f level of theory, where LANL08f is the relativistic core potential and corresponding triple-ζ valence basis set of Roy *et al.*, supplemented with a polarization f function, chosen for the metal ion [63,64].

There are three possible sequences of bonded sulfurs for the *fac* isomers: S_{te}–S_{te}–S_{te}, S_{te}–S_{te}–S_{tph}, and S_{te}–S_{thp}–S_{te}, where S_{te} and S_{thp} stand for a thioether and a thiophene type of sulfur, respectively. Only S_{te}–S_{te}–S_{tph} is relevant at r.t. During optimization of these types of structures, six different conformations of the crown thioether could be found. For each crown thioether conformation, there are three *fac* geometrical isomers, according to the positions of the monodentate ligands (plus the optical isomers, which need not be taken into account for calculation purposes). Only one of conformations is relevant at r.t., with almost 100% of combined abundance. This conformation is the same observed in the X-ray crystal structure of the optical isomer of II, previously determined by Cheu [25]. The three geometrical isomers (I–III) are represented in figure 5 [65].

After coordinate transformation of the X-ray crystal structure, to achieve the "correct" optical isomer, its comparison with II gives a heavy-atom RMSD of 0.094 Å. Since the lower frequency of vibration in these conformers corresponds mainly to the rotation of DMSO along the Ru–S bond and was found to occur at 40 cm^{-1} or less, the position of DMSO substituents should be very flexible at r.t. Neglecting such substituents significantly improves the RMSD to 0.073 Å. These results substantiate the ability of DFT to adequately reproduce the molecular structures of coordination compounds and mimic their crystal structures.

The main bond lengths and angles for isomers I–III are summarized in table 3. Bond angles of the coordination sphere show only small deviations from an octahedral geometry. The larger deviation is on the longitudinal axis, where ∢ $S_{thp–Ru–X}$ = 171–172° (X = Cl, DMSO), with S_{thp} slightly deviated to the side of its coordinated S_{te} neighbor. Ru–S bond lengths are significantly influenced by the ligand in the *trans* position. There is a strong

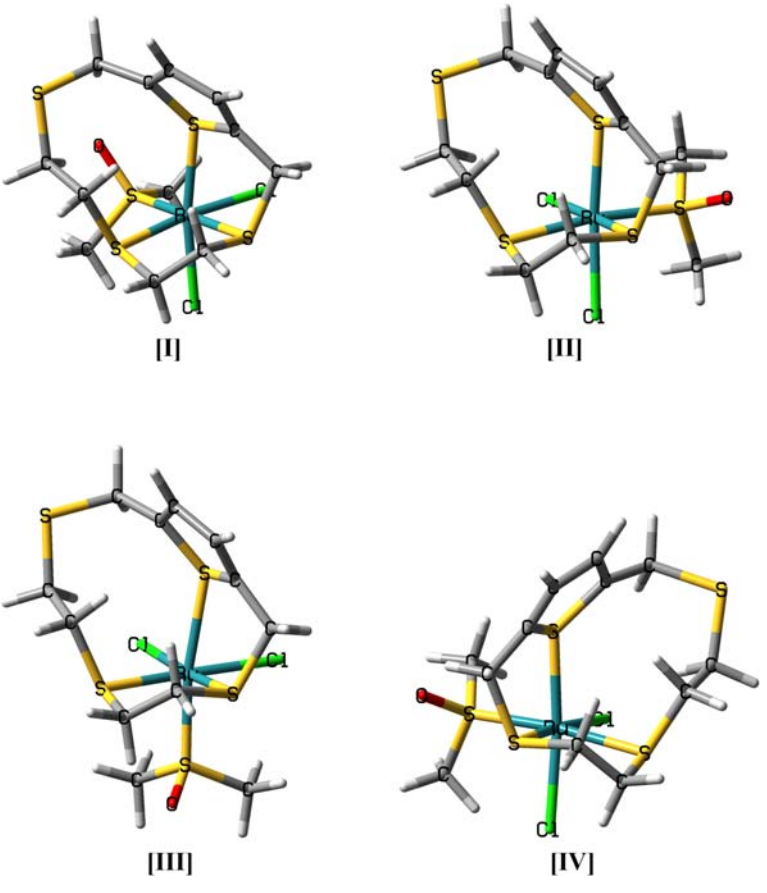

Figure 5. DFT-minimized structures of *fac*-[$RuCl_2$(DMSO)(k^3-(S_3,S_6,S_{14}-ttbt)], **5**, isomers ([I]–[III]) and X-ray crystal structure ([IV]) of the optical isomer of [II].

Table 3. Bond lengths (Å) and angles (°) of the isomers of *fac*-[$RuCl_2$(DMSO)(ttbt)], **5**.

	I	II	III	X-ray[25]
Ru–S_{thp}	2.436	2.415	2.544	2.320(2)
Ru–S_{te}[a]	2.416	2.430	2.398	2.375(2)
Ru–S_{te}[b]	2.394	2.385	2.384	2.300(2)
Ru–S_{DMSO}	2.329	2.345	2.280	2.290(2)
Ru–Cl[c]	2.431	2.432	2.465	2.400(2)
Ru–Cl[d]	2.463	2.459	2.451	2.430(2)
S_{ax}–Ru–X	170.8	171.8	171.1	172.0
S_{eq}–Ru–S_{eq}	88.2	88.2	88.4	88.4

[a]*Trans* to S_{DMSO}.
[b]*Trans* to Cl.
[c]*Trans* to S_{thp}.
[d]*Trans* to S_{te}; X = Cl, DMSO.

increase in Ru–S_{thp} from 2.42–2.44 Å to 2.54 Å when changing from a chloro to a DMSO, while Ru–S_{te} goes from 2.38–2.40 Å to 2.42–2.43 Å under the same conditions. Simultaneously, Ru–Cl goes from 2.43 Å to 2.45–2.47 Å when a *trans* S_{thp} is replaced by a S_{te}. This indicates that S_{te} are weaker π-acceptors than S_{DMSO} and that S_{thp} is even weaker than S_{te}.

The *fac* isomer III shows the longest Ru–S_{thp} bond (table 3). That would seem to indicate a decrease in the tension on the coordinated macrocycle. Nevertheless, the ruthenium bond angles permit to conclude that no such tension exists in any of the three forms. Isomer III corresponds to the only one where all bond positions with π-acceptor characteristics are *trans* to ligands which do not compete in such a way for electron density: DMSO is *trans* to S_{thp} and S_{te} are *trans* to Cl. That has a direct impact on the bond lengths. On average, the electron donors Cl and S_{thp} increase their metal bond lengths by 0.012 and 0.119 Å, respectively, while electron acceptors S_{te} and DMSO show a decrease in 0.015 and 0.057 Å, respectively.

The electronic energy and scaled thermodynamic variables, as well as isomer abundance, are indicated in table 4. At 298 K, isomer III shows *G* values at 4.6 and 4.9 kJ mol^{-1} below I and II, respectively. Isomer composition in the gas phase at r.t. was determined using a Boltzmann distribution of Gibbs free energy, with approximately 77% of III, 12% of I, and 11% of II.

Structures I–III have the same crown thioether conformation with minimal internal deviations (RMSD $\leqslant$ 0.09 Å; heavy atoms) and, at the same time, very different from the free crown thioether-minimized structure (RMSD $\approx$ 3 Å), as can be seen in figure S4. The energy required for ttbt rearrangement to the same positions of I–III corresponds to the "pre-organization energy". It was determined for single points of the three isomers at the B3LYP/6-311+G(2d,p)/LANL08f level and measured 36.4, 36.5, and 32.5 kJ mol^{-1}, respectively. These data indicate that III is expected to be favored both kinetically and thermodynamically, at least in the gas phase.

Since the solubility of the three isomers should not be too different, and the crystal structure is dictated by forces acting at the molecular level, the fact that form II is observed in the crystal phase indicates that such interactions are more relevant in II, altering the energy order compared with the one observed in the gas phase. This is plausible since the lattice energy of a molecular crystal is significantly larger than the differences observed in I–III [66]. Furthermore, atoms that induce polarity and are able to establish hydrogen bonds have a larger contribution to the lattice energy than the carbon skeleton, and it is expected that the location of DMSO and chloro atoms, which are positioned differently relative to ttbt in the three isomers, will be the relevant variable [66].

The HOMO, HOMO-1, and HOMO-2 orbitals main composition include one "t_{2g} type" orbital from the metal ion (d_{xy}, $d_{xz,}$ and d_{yz}) and p orbitals of the chloro ligands. The LUMO has contributions from d_{z2}, a p orbital from sulfur of DMSO and a π orbital delocalized over thp. The LUMO+1 is mainly composed of d_{x2-y2} from Ru(II) and p orbitals

Table 4. Energy, thermodynamic variables and composition of *cis*,*fac*-[$RuCl_2$(DMSO)(ttbt)], **5**, isomers for minimized structures at the B3LYP/6-311+G(2d,p)/LANL08*f* level.

	E (E_h)	ΔE (kJ mol^{-1})	*H* (E_h)	ΔH (kJ mol^{-1})	*S* (J mol^{-1} K^{-1})	G_{298} (E_h)	ΔG (kJ mol^{-1})	χ_i (%)
I	−3550.251303	2.84	−3549.916286	2.59	708.616	−3549.996756	4.61	12.0
II	−3550.250720	4.37	−3549.915790	3.84	711.883	−3549.996631	4.94	10.6
III	−3550.252385	0.00	−3549.917253	0.00	715.573	−3549.998513	0.00	77.4

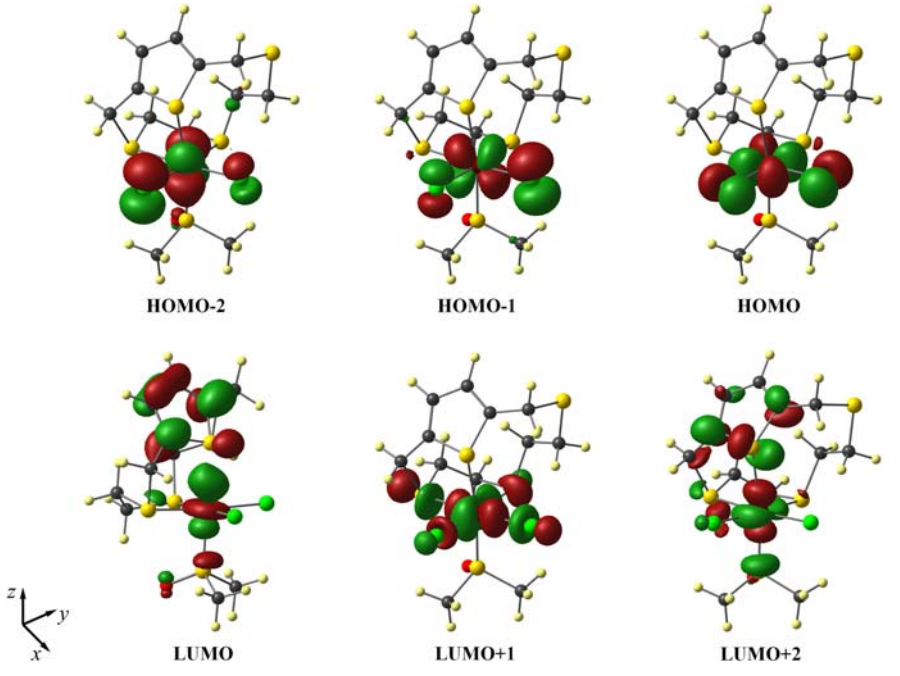

Figure 6. Contour plots at 0.05 au of HOMO-2 to LUMO+2 orbitals of the isomer [III] of **5**: optimization at the B3LYP/6-311+G(2d,p)/LANL08f level and representation with ChemCraft.

of chloro and S_{te}. HOMO-2 to LUMO+2 of III are represented in figure 6. The frontier orbitals of I and II are very similar to the analogs of III but show some differences in energy. The HOMO-LUMO gap decreases from I to III, presenting the following values 27,500, 26,800, and 26,600 cm^{-1}, respectively.

2.6. *Solubility and reactivity*

Compounds **3**, **4,** and **6** are reasonably soluble in the majority of solvents because of their ionic nature; neutral **2** and **5** are weakly soluble, except in DMSO or DMF, and water in the case of **2**.

The labilities of **1–3** were tested in polar coordinating solvents CH_3CN, DMSO, and water. The reflux of **1** in CH_3CN does not result in any change of the coordination sphere, even when NH_4PF_6 is added. This contrasts with aqueous solution results, under an excess of chloride, where *O*-DMSO dissociation occurs [67].

fac-[$RuCl_2$(DMSO)([9]aneS_3)], **2**, shows no reaction in CH_3CN even under prolonged reflux, while solubilization in DMSO-d_6, followed by ^{1}H NMR for 24 h, shows no signs of exchange of chloro for DMSO-d_6. Exchange of DMSO for DMSO-d_6 is observed instead, as previously reported for [$RuCl_2$(DMSO)(tpy)] [68]. Nevertheless, adding an equimolar amount of NH_4PF_6 to CH_3CN resulted in formation of [RuCl(CH_3CN)(DMSO)([9]aneS_3)]PF_6, **7** (73% yield). Since Ru(II) prefers a dissociative substitution mechanism [69] and PF_6^- increases the reactivity of **2** in CH_3CN, a five-coordinate intermediate is plausible, stabilized by the non-coordinating PF_6^-. A similar situation was recently described by Izquierdo *et al.*, where the reaction was followed by ESI-MS [33]. When **2** is solubilized in water, followed by addition of NH_4PF_6, a solid compound precipitates that

gives $[Ru(CH_3CN)_3([9]anoS_3)](PF_6)_2$ (77%) after solubilization in CH_3CN. This complex has been previously described by Landgrafe and Sheldrick [28].

When *cis*-[RuCl(DMSO)([12]aneS$_4$)]Cl, **3**, is heated in CH_3CN under reflux for 5 h, it does not change its composition. If **3** is solubilized in CH_3CN in the presence of NH_4PF_6, the only modification that occurs is the counter-ion exchange from Cl^- to PF_6^-. But, when the reaction is performed in CH_3CN/water, with NH_4PF_6 in equimolar amount, the complex *cis*-[RuCl(CH_3CN)([12]aneS$_4$)]PF_6 is formed with an 89% yield [30]. In a similar experiment, **3** was solubilized in water with a large excess of NaBr and heated for several hours, followed by evaporation, solubilization in CH_3CN, filtration (to remove salt) and overnight reflux. Raman spectroscopy identified the isolated compound as *cis*-[RuCl(CH_3CN)([12]aneS$_4$)]$^+$, probably in the bromide form. Such results confirm that the Ru–Cl bond of **3** is quite inert, with exchange typically taking place in the DMSO position [30]. So far, removing the chloro has been possible only with chelate ligands or good halogen abstractors [30,70]. This supports the restricted ability of thioethers to neutralize positive charges by σ donation [44,71].

Summarizing, these studies confirm that **2** and **3** have chloro ligands that are resistant to coordinating solvents like CH_3CN or DMSO. The presence of water significantly increases the reactivity of **2**, with all monodentate positions being able to be exchanged, while in **3** only DMSO labilization occurs. Detailed hydrolysis studies are underway for some of these complexes and will be published separately.

3. Experimental

3.1. *General data and physical measurements*

All complexes were prepared under argon using Schlenk techniques. The solvents were *p.a.* or superior quality. Ultra-pure water was used for aquation studies. Chemicals were acquired from established international suppliers and used without purification.

Elemental analyzes (C, H, N, and S) were performed on a Leco CHNS-932 (Chemistry Department, Aveiro University). The infrared spectra (4000–200 cm^{-1}) were acquired on a FTIR Mattson-7000 Galaxy series spectrometer (2 cm^{-1} resolution), with material dispersed in KBr ($\geqslant$400 cm^{-1}) or CsI ($\geqslant$200 cm^{-1}) pellets, while Raman spectra were acquired on a Bruker RFS 100/S FT spectrometer, with Nd/YAG laser excitation (1064 nm). NMR spectra in solution were registered on 300 or 500 MHz Bruker DRX spectrometers. All chemical shifts refer to TMS or residual proton signals of the solvents. The solid-state ^{13}C-CP-MAS and ^{13}C-HP Dec-MAS spectra were obtained on a Bruker ARX spectrometer operating at 400 MHz (100.6 MHz for ^{13}C) using glycine as internal standard. The UV/Vis spectra were obtained on a Jasco V-560 spectrophotometer at 20°C. ESI-MS spectra were acquired with a Micromass Q-TOF-2 (Micromass, Manchester) with a Z-spray API source. The nominal mass resolution was set at 8000. 50 : 50 and 40 : 60 water/methanol mixtures were employed as eluents for **6** and **7**, respectively. The capillary needle voltage was 3 kV, and the cone voltage applied was in the range of 10–60 V.

3.2. *Theoretical calculations*

All calculations were performed on the bach.vcu.edu cluster at the Center for High Performance Computing (VCU) using the Gaussian® 03 program [72], version D2. The "Bach" cluster consists of a total of 764 AMD Opteron™ 64-bit cores, each with a minimum of

2 GB/core RAM, 14 TB internal disk storage, 1 TB total RAM, 2 TB of /home space, and /tmp space of 50–164 GB per node. Networking infrastructure is gigabit Ethernet.

SCF convergence requested 10^{-8} on the root-mean-square density matrix, 10^{-6} on maximum deviation on the density matrix and 10^{-6} on the energy. DFT optimization requested fine grid accuracy (10^{-7} for energy and 10^{-6} for gradient).

Ttbt optimizations were performed for HF and B3LYP methods using the following basis sets: 3-21G*, 6-31G(d), 6-31+G(d), 6-31+G(d,p), 6-31+G(2d,p), 6-311G(d), 6-311+G(d), 6-311+G(d,p), 6-311+G(2d,p), and 6-311++G(2d,p). The results permitted to select B3LYP/6-311+G(2d,p) as the more adequate model, which was subsequently used in the coordination compound calculations.

Chem3D® Ultra v.8.0 program was used to build **5** isomers and their conformers, using its ability to introduce lone pairs in sulfur with selected *exo*/*endo* orientation. MM2-minimized structures can then lock local minima that were used as input for further calculations at the B3LYP/6-31G(d)/LANL08f level that corresponds to an intermediate quality model, the results of which were fed to the more accurate B3LYP/6-311+G(2d,p)/LANL08f. LANL08f is the triple-ζ valence basis set and relativistic core potential of Roy *et al.* [63]. It is a recent revision of the classic Hay and Wadt LANL2DZ [73] and includes a new contraction of the basis sets, which is more suited to DFT calculations than the previous double ζ contractions, which were based upon Hartree–Fock atomic results. It is also supplemented with a polarization f function that corresponds to the single primitive determined by Frenking and co-workers [64]. Despite the fact that its exponents have not originally been optimized for DFT, they are seldom used because of its good behavior [63].

The final model is able to deal with long-range interactions caused by stereochemical hindrance and diffuse orbitals interaction for sulfur, chloro, and ruthenium (nephelauxetic effect). For models with B3LYP/6-311+G(2d,p), or better quality, the scaling factors are known to achieve convergence, even in more difficult cases (as polarized hydrogens bonded to electronegative atoms) permitting a better thermodynamic data prediction [74,75]. Scaling factors at 298 K for ΔH_{vib} (1.0040) and S (1.0094) were taken from Merrick *et al.* [75]. The mole fractions, X_i, for the three isomers were determined from the difference in Gibbs free energy, ΔG_i, using the Boltzmann distribution law, that is, $X_i = \exp(-\Delta G_i/RT)/[\Sigma_j \exp(-\Delta G_j/RT)]$, and the most stable isomer as energy reference.

Minimized structures correspond to local minima in the potential energy surface, since no negative values were found on their vibrational determined frequencies.

Fractional to Cartesian coordinates conversion in the tetragonal crystal system of **5**, determined by E.L.S. Cheu, was carried out with the crystallographic tool of ChemCraft [76]. For representation purposes, the hydrogens were inserted automatically in GaussView [77] since they are absent in the solved crystal structure. Besides ChemCraft and Gauss View, PyMol was also used as visualization/graphic program [78].

3.3. *Syntheses*

The complexes *fac*-[$RuCl_2$(DM***S***O)$_3$(DMS***O***)] (**1**), *fac*-[$RuCl_2$(DM***S***O-d_6)$_3$(DMS***O***-d_6)] (**1a**), [$RuCl_2$(DMSO)([9]aneS_3)] (**2**), *cis*-[RuCl(DMSO)([12]aneS_4)]Cl (**3**), *cis*-[RuCl(DMSO)([14]aneS_4)]PF_6 (**4**), [Ru([9]aneS_3)$_2$](PF_6)$_2$, and [Ru(CH_3CN)$_3$([9]aneS_3)](PF_6)$_2$ were prepared according to the literature [15,28,30,34,79].

The synthesis and characterization of the fully deuterated DMSO derivatives of **1**, **2,** and **3**, as well as the bromo and iodo analogs of **2**, are presented in Supplementary Material.

***fac*-[$RuCl_2$(DMSO)(ttbt)] (5)** – One mmol of [$RuCl_2(DMSO)_4$] (485 mg) and one of 3,6,9,14-tetrathia-bicyclo[9.2.1]tetradeca-1(13),11-diene, *ttbt* (263 mg), were mixed in absolute ethanol and heated at reflux for 4 h, with the mixture acquiring a brown color. After cooling, the suspension was kept at −20 °C for 48 h. The solid was collected by filtration under vacuum and washed with cold ethanol and diethyl ether. After 2 h drying at 70°C, it was suspended in 75 mL of water and extracted with chloroform until the extract showed no color (200 mL). After concentration on the rotary evaporator (40 mL), the remaining solvent was slowly evaporated in the fume hood. The solid was dried at 70°C (yield: 130 mg; 25%). Anal. Calcd for $C_{12}H_{30}Cl_2ORuS_5 \cdot 0.2$ DMSO $\cdot$ 0.25 $CHCl_3$ (%): C, 27.2; H, 3.9; S, 29.9. Found: C, 27.2; H, 3.8; S, 29.9. Another sample gave: Anal. Calcd for $C_{12}H_{30}Cl_2ORuS_5 \cdot 0.4$ DMSO $\cdot$ 0.4 $CHCl_3$ (%): C, 26.8; H, 3.9; S, 29.3. Found: C, 26.6; H, 3.9; S, 29.3.

^{1}H NMR – δ_H ($CDCl_3$), ppm: 7.11 (1H, d; thiophene), 7.06 (1H, d; thiophene) [4.50–3.55] and [3.10–2.50] (12H, d + m, CH_2 of *ttbt*); 3.50 (3H, s, CH_3 of DMSO), 3.43 (3H, s, CH_3 of DMSO). **FT-IR** (KBr, cm^{-1}): 3058 (ν_{C-H} aromatic), 3000 sh (ν_{C-H} DMSO), 2962 (ν_{C-H} CH_2 of *ttbt*), 2916 (ν_{C-H}), 1873 + 1862, 1491 ($\nu_{C=C}$ thiophene), 1410 + 1384 sh (δ_{C-H}), 1304 + 1292, 1251 + 1237, 1212, 1165, 1087 ($\nu_{S=O}$), 1016 (ρ_{C-H}), 969, 926, 871, 821, 721 (ν_{C-S}), 681 (ν_{C-S}), 649, 573, 487 + 468 + 432 (ν_{Ru-S}), 412 sh, 380 (δ_{C-S-O}), 293. **FT-Raman** (cm^{-1}): 3064, 3004, 2964, 2919, 2832, 1493, 1475 sh, 1416, 1332, 1235, 1172, 1104, 1019, 860, 804, 731, 716, 682, 647, 637, 575, 488 + 468 + 432 (ν_{Ru-S}), 413 sh, 380, 360–300 several peaks, 293, 277 + 246 br (ν_{Ru-Cl}), 206, 186, 135, 107 *sh*. **UV/Vis** – (DMF) λ_{max}, nm ($\varepsilon \times 10^{-3}$ M^{-1} cm^{-1}): 415 (1.7), 319 sh (4.7), 274 (15.1).

[RuCl(DMSO)([14]aneN$_4$)]PF_6 (6) – Two mmol of [$RuCl_2(DMSO)_4$] (969 mg) and two mmol of [14]aneN$_4$ (400 mg) were mixed in absolute ethanol and heated at reflux for 4 h. The mixture darkens gradually until a final dark brown color is observed. After cooling, a slight excess of NH_4PF_6 was added (4.2 mmol) with immediate precipitation. The mixture was kept at −20°C for 48 h, after which it was filtered under vacuum and a dark brown viscous material was obtained. Adding CH_3CN allows the soluble brown fraction to be separated from a yellow solid that was collected. The filtrate was evaporated until oil was formed. A small amount of fresh CH_3CN results in a new fraction of the yellow precipitate. Both solid fractions were solubilized in acetone and filtered under vacuum to remove an almost white solid. The filtrate was evaporated to dryness and dried at 65°C (yield: 481 mg; 43%).

^{1}H NMR – δ_H (CD_3NO_2), ppm: 8.56, 8.37, 8.30 and 8.08 (N*H*, s), [3.65–3.40] (2H, m, CH_2), 3.32 (3H, s, DMSO), 3.27 (3H, s, DMSO), [3.25–3.0] (6H, m, CH_2), [3.0–2.7] (6H, m, CH_2), [2.7–2.55] (2H, m, CH_2), [2.3–1.7] (4H, m, CH_2). **FT-IR** (cm^{-1}, KBr): 3313, 3218, 3191 and 3153 (ν_{N-H}), 3096, 2974, 2959, 2924 + 2917, 2876 and 2859 (ν_{C-H}), 1456, 1423, 1400, 1365, 1301, 1281, 1246, 1228, 1206, 1186, 1127 and 1106 (δ_{C-H}), 1069 + 1061 sh, 1043 + 1035, 1009, 957, 844 (PF_6^-), 740, 713, 558 (PF_6^-), 494, 478, {442 and 424 sh} (ν_{Ru-S}), 395, 379 (δ_{C-S-O}), 304, 280 (ν_{Ru-Cl}), 258. **FT-Raman** (cm^{-1}): {3312, 3218, 3185 and 3159} (ν_{N-H}), 3027, 2993, 2977, 2965, 2942 + 2934, 2882 and 2860 (ν_{C-H}), 1481 (δ_{N-H}), 1458, 1445, 1381, 1281, 1250, 1137 and 1097 (δ_{C-H}), 1081 ($\nu_{S=O}$), 1042, 1013 (δ_{C-H}), 1001, 958, 864, 847, 833, 801, 741 (PF_6^-), 717 and 684 (ν_{C-S}), 444 (ν_{Ru-S}), 412, 397 (δ_{C-S-O}), 333, 315, 282 (ν_{Ru-Cl}), 266, {253 and 239} (ν_{Ru-N}), 215, 194, 182, 145. **ESI-MS** (H_2O/MeOH 1 : 1): m/z = 415, $[M]^+$ ≡ $[RuCl(DMSO)([14]aneN_4)]^+$; 377, $[M\text{-}Cl]^+$; 299, $[M\text{-}Cl\text{-}DMSO]^+$.

[RuCl(CH_3CN)(DMSO)([9]aneS_3)]PF_6 (7) – One mmol of [$RuCl_2$(DMSO)([9]aneS_3)] (430 mg) was added to 50 mL of CH_3CN and heated at reflux for 2 h. 163 mg of NH_4PF_6 (1 mmol) was solubilized in 20 mL of CH_3CN and added to the reaction. After 15 min, a color change from orange to yellow was observed. Simultaneously, a white material settled down, which was removed by filtration. The filtrate was concentrated to 10 mL and left standing to evaporate slowly at room temperature. Orange crystals form after 24 h, while yellow flocculates can be collected at higher concentration. The two fractions can easily be separated in diethyl ether after sonication, since the denser, orange fraction settles down, while the yellow fraction stays suspended. After collection the yellow fraction was washed with diethyl ether and dried at 70°C, while the orange one was washed with diethyl ether, solubilized in acetone, evaporated in a rotary evaporator and dried. Both fractions correspond to the same compound (yield: 424 mg; 73%).

^{1}H NMR – δ_H (acetone-d_6), ppm: 3.36 (6H, s, DMSO), [3.25–2.75] (12H, m, CH_2), 2.67 (3H, s, CH_3CN). **FT-IR** (cm^{-1}, KBr): 2997, 2958, 2938 and 2910 (ν_{C-H}), 2314 and 2287 ($\nu_{C\equiv N}$), 1454, 1410, 1361, 1315, 1298, 1184, 1173 + 1167, 1118 (δ_{C-H}), 1101 + 1092 ($\nu_{S=O}$), 1032, 977, 941, 921, 911, 842 (PF_6^-), 742, 720, 685, 662, 623, 558 (PF_6^-), {493, 460 and 430} (ν_{Ru-S}), 377 (δ_{C-S-O}), 352, 340, 297, 256, 247 (ν_{Ru-Cl}). **FT-Raman** (cm^{-1}): 3012 sh, 2999, 2984, 2959 sh, 2939, 2918 and 2911 (ν_{C-H}), 2314 and 2286 ($\nu_{C\equiv N}$), 1455, 1420 + 1412, 1363, 1316, 1298, 1185, 1173, 1138, 1128, 1119 (δ_{C-H}), 1100 + 1091 ($\nu_{S=O}$), 1032, 1017, 1009, 994, 977, 947, 912, 741 (PF_6^-), 720, 684, 662, 620, 567, {496, 461 and 428} (ν_{Ru-S}), 377 (δ_{C-S-O}), 353, 340, 311, 299, 284, 269, 248 (ν_{Ru-Cl}), 224 (ν_{Ru-N}), 211, 191, 173, 145, 127, 101. **ESI-MS** (H_2O/MeOH 2 : 3): m/z = 435, $[M]^+ \equiv$ [RuCl(CH_3CN)(DMSO)([9]aneS_3)]$^+$; 412.9, $[M - CH_3CN + H_2O]^+$; 394.9, $[M - CH_3CN]^+$.

4. Concluding remarks

Seven ruthenium(II)–chloro–dimethylsulfoxide complexes were prepared and characterized. Previously known **1–4** were further characterized at the spectroscopic level and their reactivity studied. Compounds **2** and **3** were studied in more detail by FT-IR, FT-Raman, and UV/Vis. Deuterated forms of **1–3** and alternative halogen derivatives of **2** were prepared to conduct a more rigorous assignment of vibrational and UV/Vis spectra. Reactivity and solubilization of such compounds in coordinating solvents (H_2O, CH_3CN, and DMSO) indicate that the chosen macrocycle controls the species found in solution, with the chloro positions of [$RuCl_2$(DMSO)([9]aneS_3)] (**2**) being more easily replaced than in *cis*-[RuCl(DMSO)([12]aneS_4)]Cl (**3**). The counter-ion has a direct impact on the reactivity, with hexafluorophosphate helping solvolysis to occur and/or favoring precipitation of the chloride salt. In fact, [RuCl(CH_3CN)(DMSO)([9]aneS_3)]PF_6 (**7**) could be isolated from a CH_3CN solution in such a way. A five-coordinate species is predicted to play a major role on solvolysis processes, probably better stabilized by the bigger counter-ion.

Besides **7**, two other new complexes of this class of compounds were presented. [$RuCl_2$(DMSO)(ttbt)] (**5**) is the first published octahedral complex of ttbt. It is coordinated by three of its four sulfurs, in a *fac* arrangement (S_{te}–S_{te}–S_{thp}) according both to X-ray crystal structure and theoretical calculations at the DFT level. NMR indicates that an equilibrium of different isomers occurs in solution that agrees with DFT results, with predicted abundances of 77% (I), 12% (II) and 11% (III) at r.t., based on a distribution of Gibbs free energy at 298 K. They correspond to different positions of chloro and DMSO in their internal relation with ttbt.

[RuCl(DMSO)([14]aneN$_4$)]PF$_6$ (**6**) is a kinetically air stable Ru(II)–polyamine complex, despite [14]aneN$_4$ high σ-donor ability and lack of available orbitals for π back donation. It shows a gradual (weeks) internal amine oxidation assisted by the ruthenium center.

Supplementary material

Synthesis and characterization of complexes **1a**, **2a**, **2b**, **2c,** and **3a** are presented in Supplementary Material. Infrared and Raman band assignments for **1**, **2** and **3**, same as their deuterated DMSO analogs are presented in table S1, while ^{1}H NMR spectra of **2** and **7** are shown in figures S1 and S2. Further details of the molecular modeling results and methodology are also included in Supplementary Material, namely in figures S3 and S4. The multi-Gaussian fitting of the convoluted electronic spectra of **2**, **2b,** and **2c** are shown in figures S5–S7.

Acknowledgements

Dr Paula Ferreira and Prof. Graça Santana-Marques (University of Aveiro) are thanked for running solid-state ^{13}C NMR and ESI-MS analysis, respectively. J.M. thanks FCT (Portugal) for a post-doc grant (SFRH/BPD/41138/2007) and the Center for High Performance Computing (VCU) for access to bach.vcu.edu cluster.

References

[1] H.-J. Küppers, K. Wierghardt, B. Nuber, J. Weiss, E. Bill, A.X. Trautwein. *Inorg. Chem.*, **26**, 3762 (1987).
[2] A.J. Blake, A.J. Holder, T.I. Hyde, M. Schröder. *J. Chem. Soc., Chem. Commun.*, 987 (1987).
[3] E.A. Abel, P.D. Beer, I. Moss, K.G. Orrell, V. Šik, P.A. Bates, M.B. Hursthouse. *J. Chem. Soc., Chem. Commun.*, 978 (1987).
[4] S.R. Cooper, S.C. Rawle. In *Structure and Bonding*, D.M.P. Mingos (Ed.), Vol. 72, pp. 1–72, Springer, Berlin/Heidelberg (1990).
[5] A.J. Blake, R.O. Gould, A. Halcrow, A.J. Holder, T.I. Hyde, M. Schröder. *J. Chem. Soc., Dalton Trans.*, 3427 (1992).
[6] (a) A.J. Blake, R.O. Gould, A.J. Holder, T.I. Hyde, A.J. Lavery, M.O. Odulate, M. Schröder. *J. Chem. Soc*., *Chem. Commun*., 118 (1987); (b) J. Clarkson, R. Yagbasan, P.J. Blower, S.C. Rawle, S.R. Cooper. *J. Chem. Soc*., *Chem. Commun*., 950 (1987); (c) A.J. Blake, R.O. Gould, A.J. Holder, T.I. Hyde, M. Schroder. *J. Chem. Soc., Dalton Trans*., 1861 (1988); (d) A.J. Blake, J.A. Greig, A.J. Holder, T.I. Hyde, A.Taylor, M. Schröder. *Angew. Chem. Int. Ed. Engl*., **29**, 197 (1990); (e) H. Nikol, H.-B. Bürgi, K.I. Hardcastle, H.B. Gray. *Inorg. Chem*., **34**, 6319 (1995); (f) L. Messori, F. Abbate, G. Marcon, P. Orioli, M. Fontani, E. Mini, T. Mazzei, S. Carotti, T. O'Connell, P. Zanello. *J. Med. Chem*., **43**, 3541 (2000).
[7] W.N. Setzer, C.A. Ogle, G.S. Wilson, R.S. Glass. *Inorg. Chem.*, **22**, 266 (1983).
[8] (a) K. Wieghardt, H.J. Kuppers, J. Weiss. *Inorg. Chem*., **24**, 3067 (1985); (b) G.S. Wilson, D.D. Swanson, R.S. Glass. *Inorg. Chem.*, **25**, 3827 (1986); (c) A.J. Blake, R.O. Gould, A. Halcrow, A.J. Holder, T.I. Hyde, M. Schröder. *J. Chem. Soc.*, *Dalton Trans*., 3427 (1992); (d) G.R. Willey, J. Palin, M.T. Lakin, N.W. Alcock. *Transition Met. Chem.*, **19**, 187 (1994); (e) G.J. Grant, S.S. Shoup, C.E. Hadden, D.G. Van Derveer. *Inorg. Chim. Acta*, **274**, 192 (1998); (f) A.L. Hector, W. Levason, A.J. Middleton, G. Reid, M. Webster. *Eur. J. Inorg. Chem*., 3655 (2007).
[9] (a) S.C. Rawle, R. Yagbasan, K. Prout, S.R. Cooper. *J. Am. Chem. Soc*., **109**, 6181 (1987); (b) J.L. Shaw, J. Wolowska, D. Collison, J.A.K. Howard, E.J.L. McInnes, J. McMaster, A.J. Blake, C. Wilson, M. Schröder. *J. Am. Chem. Soc.*, **128**, 13287 (2006).
[10] (a) K. Dalley, J.S. Smith, S.B. Larson, K.L. Matheson, J.J. Christensen, R.M. Izatt. *J. Chem. Soc*., *Chem. Commun.*, 84 (1975); (b) R.E. de Simone, M.D. Glick. *J. Am. Chem. Soc.*, **98**, 762 (1976); (c) R.E. Wolf Jr., J.R. Hartman, J.M.E. Storey, B.M. Foxman, S.R. Cooper. *J. Am. Chem. Soc*., **109**, 4328 (1987); (d) G.H. Robinson, S.A. Sangokoya. *J. Am. Chem. Soc.*, **110**, 1494 (1988); (e) P. Comba, A. Fath, A. Kuhner, B. Nuber. *J. Chem. Soc.*, *Dalton Trans*., 1889 (1997).

[11] P. Bultinck, A. Huyghebaert, C. Van Alsenoy, A. Goeminne. *J. Phys. Chem. A*, **105**, 11266 (2001).
[12] D.J. White, H.-J. Küppers, A.J. Edwards, D.J. Watkin, S.R. Cooper. *Inorg. Chem.*, **31**, 5351 (1992).
[13] S.O.C. Matondo, P. Mountford, D.J. Watkin, W.B. Jondes, S.R. Cooper. *J. Chem. Soc., Dalton Trans.*, 161 (1995).
[14] (a) B. Serli, E. Zangrando, T. Gianferrara, C. Scolaro, P. Dyson, A. Bergamo, E. Alessio. *Eur. J. Inorg. Chem*., 3423 (2005); (b) R. Bieda, M. Dobroschke, A. Triller, I. Ott, M. Spehr, R. Gust, A. Prokop, W.S. Sheldrick. *ChemMedChem*, **5**, 1123 (2010); (c) I. Bratsos, E. Mitri, F. Ravalico, E. Zangrando, T. Gianferrara, A. Bergamo, E. Alessio. *Dalton Trans*., **41**, 7358 (2012).
[15] M. Pillinger, I.S. Gonçalves, A.D. Lopes, J. Madureira, P. Ferreira, A.A. Valente, T.M. Santos, J. Rocha, J.F. S. Menezes, L.D. Carlos. *J. Chem. Soc., Dalton Trans.*, 1628 (2001).
[16] J. Pickardt, L. von Chrzanowski, R. Steudel, M.Z. Borowski. *Naturforsch. B*, **59**, 1077 (2004).
[17] H. Adams, A.M. Amado, V. Félix, B.E. Mann, J. Antelo-Martinez, M. Newell, P.J.A. Ribeiro-Claro, S. Spey, J.A. Thomas. *Chem. Eur. J*., **11**, 2031 (2005).
[18] (a) B. Patel, G. Reid. *J. Chem. Soc.*, *Dalton Trans.*, 1303 (2000); (b) A.J. Barton, N.J. Hill, W. Levason, G. Reid. *J. Chem. Soc*., *Dalton Trans*., 1621 (2001); (c) J. Madureira, T.M. Santos, C.M.F. Barros, F.M.L. Amado, M.G. Santana-Marques, A.J. Ferrer-Correia. *Adv. Mass Spectrom*., **15**, 737 (2001); (d) S. Du, J.A. Kautz, T.D. McGrath, F.G.A. Stone. *J. Chem. Soc*., *Dalton Trans*., 2791 (2001); (e) N.R. Brooks, A.J. Blake, N.R. Champness, P.A. Cooke, P. Hubberstey, D.M. Proserpio, C. Wilson, M. Schröder. *J. Chem. Soc*., *Dalton Trans*., 456 (2001); (f) C.D. Beard, L. Carr, M.F. Davis, J. Evans, W. Levason, L.D. Norman, G. Reid, M. Webster. *Eur. J. Inorg. Chem*., 4399 (2006); (g) N. Shan, H. Adams, J.A. Thomas. *Inorg. Chim. Acta*, **359**, 759 (2006); (h) M.L. Helm, L.L. Hill, J.P. Lee, D.G. Van Derveer, G.J. Grant. *Dalton Trans*., 3534 (2006); (i) M.F. Davis, W. Levason, M.E. Light, R. Ratnani, G. Reid, K. Saraswat, M. Webster. *Eur. J. Inorg. Chem*., **13**, 1903 (2007); (j) C. Gurnani, M. Jura, W. Levason, R. Ratnani, G. Reid, M. Webster. *Dalton Trans*., 1611 (2009); (k) S.-C. Chan, H.-Y. Cheung, C.-Y. Wong. *Inorg. Chem*., **50**, 11636 (2011). *For references previous to 2000, see Supplementary Material.*
[19] E. Weber, F. Voegtle. *Justus, Liebigs Ann. Chem.*, 891 (1976).
[20] C.R. Lucas, L. Shuang, M.J. Newlands, J.P. Charland, E.J. Gabe. *Can. J. Chem.*, **66**, 1506 (1988).
[21] C.R. Lucas, S. Liu, M.J. Newlands, E. Gabe. *Can. J. Chem.*, **68**, 1537 (1990).
[22] S. Liu, C.R. Lucas, M.J. Newlands, J.-P. Charland. *Inorg. Chem.*, **29**, 4380 (1990).
[23] (a) R. Blom, D.W.H. Rankin, H.E. Robertson, M. Schröder, A. Taylor. *J. Chem. Soc*., *Perkin Trans. 2*, 773 (1991); (b) J.C. Lockhart, D.P. Mousley, G.A. Forsyth, F. Teixidor, M.P. Almajano, L. Escriche, J. Casabo, R. Sillanpa, R. Kivekas. *J. Chem. Soc*., *Perkin Trans*. *2*, 1309 (1994); (c) S.E. Hiller, D. Feller. *J. Phys. Chem. A*, **104**, 652 (2000); (d) B. Jagannadh, S.S. Reddy, R.P. Thangavelu. *J. Mol. Model.*, **10**, 55 (2004).
[24] T. Rambusch, K. Hollman-Gloe, K. Gloe. *J. Prakt. Chem.*, **341**, 202 (1999).
[25] E.L.S. Cheu. Thioether and sulfoxide complexes of ruthenium; preliminary in vitro studies of water-soluble species. PhD Thesis, University of British Columbia, Canada (2000).
[26] (a) N. Farrell. *Transition Metal Complexes as Drugs and Chemotherapeutic Agents*, p. 291, Kluwer Academic, Boston, MA (1989); (b) G. Sava, A. Bergamo. In *Platinum and Other Heavy Metal Compounds in Cancer Chemotherapy: Molecular Mechanisms and Clinical Applications*, A. Bonetti, R. Leone, F.M. Muggia, S.B. Howell (Eds.), pp. 57–66, Humana Press, New York, NY (2009); (c) J.C. Dabrowiak. In *Metals in Medicine*, pp. 149–189, Wiley, Chichester (2009).
[27] N. Farrell. *J. Chem. Soc., Chem. Commun.*, 331 (1982).
[28] C. Landgrafe, W.S. Sheldrick. *J. Chem. Soc., Dalton Trans.*, 1885 (1994).
[29] B. de Groot, H.A. Jenkins, S.J. Loeb, S.L. Murphy. *Can. J. Chem.*, **73**, 1102 (1995).
[30] T.M. Santos, B.J. Goodfellow, J. Madureira, J.P. de Jesus, V. Félix, M.G.B. Drew. *New J. Chem.*, **23**, 1015 (1999).
[31] E. Iengo, E. Zangrando, E. Baiutti, F. Munini, E. Alessio. *Eur. J. Inorg. Chem.*, 1019 (2005).
[32] (a) B.J. Goodfellow, V. Félix, S.M.D. Pacheco, J.P. de Jesus, M.G.B. Drew. *Polyhedron*, **15**, 393 (1996); (b) B.J. Goodfellow, S.M.D. Pacheco, J.P. de Jesus, V. Félix, M.G.B. Drew. *Polyhedron*, **16**, 3293 (1997); (c) J. Madureira, T.M. Santos, B.J. Goodfellow, M. Lucena, J.P. de Jesus, M.G. Santana-Marques, M.G.B. Drew, V. Félix. *J. Chem. Soc.*, *Dalton Trans.*, 4422 (2000); (d) T.M. Santos, J. Madureira, B.J. Goodfellow, M.G.B. Drew, J.P. de Jesus, V. Félix. *Met. Based Drugs*, **8**, 125 (2001); (e) M.G.O. Santana-Marques, F.M.L. Amado, A.J. Ferrer-Correia, M. Lucena, J. Madureira, B.J. Goodfellow, V. Félix, T.M. Santos. *J. Mass Spectrom*., **36**, 529 (2001); (f) C.S. Araújo, M.G.B. Drew, V. Félix, L. Jack, J. Madureira, M. Newell, S. Roche, T.M. Santos, J.A. Thomas, L. Yellowlees. *Inorg. Chem.*, **41**, 2250 (2002); (g) C. Nunes, M. Pillinger, A. Hazell, J. Jepsen, T.M. Santos, J. Madureira, A.D. Lopes, I.S. Gonçalves. *Polyhedron*, **22**, 2799 (2003); (h) R.A. Izquierdo, C.M.F. Barros, F.M.L. Amado, M.G.O. Santana-Marques, A.J. Ferrer-Correia, J. Madureira, T.M. Santos, V. Félix. *Int. J. Mass Spectrom.*, **243**, 257 (2005).
[33] R.A. Izquierdo, J. Madureira, C.I.V. Ramos, M.G.O. Santana-Marques, T.M. Santos. *Int. J. Mass Spectrom.*, **301**, 143 (2011).
[34] I.P. Evans, A. Spencer, G. Wilkinson. *J. Chem. Soc., Dalton Trans.*, 204 (1973).
[35] C.R. Lucas, L. Shuang, M.J. Newlands, J.-P. Charland, E.J. Gabe. *Can. J. Chem.*, **67**, 639 (1989).

[36] J.P.L. Madureira, Ruthenium complexes with polythioether and/or polypyridyls: Synthesis, structural characterization and DNA interactions. PhD Thesis, Universidade de Aveiro, Portugal (2005).
[37] E.L.S. Cheu (2000), Thioether and sulfoxide complexes of ruthenium: Preliminary in vitro studies of water-soluble species. Available online at: https://circle.ubc.ca/handle/2429/11397?show=full (accessed 17 May 2012).
[38] (a) V.C. Lau, L.A. Berben, J.R. Long. *J. Am. Chem. Soc.*, **124**, 9042 (2002); (b) L.A. Berben, M.C. Faia, N. R.M. Crawford, J.R. Long. *Inorg. Chem*., **45**, 6378 (2006); (c) P.J. Barnard, R.S. Vagg. *J. Inorg. Biochem.*, **99**, 1009 (2005); (d) L.A. Berbern, M.C. Faia, R.M. Crawford, J.R. Long *Inorg. Chem*., **45**, 6378 (2006).
[39] C.-K. Poon, C.-M. Che. *J. Chem. Soc., Dalton Trans*., 756 (1980).
[40] C.-K. Poon, C.-M. Che. *Inorg. Chem.*, **20**, 1640 (1981).
[41] D.D. Walker, H. Taube. *Inorg. Chem.*, **20**, 2828 (1981).
[42] K. Sakai, Y. Yamada, T. Tsubomura. *Inorg. Chem.*, **35**, 3163 (1996).
[43] R.F. Keene. *Coord. Chem. Rev.*, **187**, 121 (1999) and cited references.
[44] C. Landgrafe, W.S. Sheldrick. *J. Chem. Soc., Dalton Trans*., 989 (1996).
[45] (a) M.N. Bell, A.J. Blake, R.M. Christie, R.O. Gould, A.J. Holder, T.I. Hyde, M. Schröder, L.J. Yellowlees. *J. Chem. Soc., Dalton Trans*., 2977 (1992); (b) J. Cannadine, A. Hector, A.F. Hill. *Organometallics*, **11**, 2323 (1992); (c) A.L. Hector, A.F. Hill. *Inorg. Chem*., **34**, 3797 (1995); (d) J.C. Cannadine, A.F. Hill, A.J.P. White, D.J. Williams, J.D.E.T. Wilton-Ely. *Organometallics*, **15**, 5409 (1996); (e) G. Laurenczy, S. Jedner, E. Alessio, P.J. Dyson. *Inorg. Chem. Commun*., **10**, 558 (2007); (f) J.C. Green, A.L. Hector, A.F. Hill, S. Lin, J.D.E.T. Wilton-Ely. *Organometallics*, **27**, 5548 (2008).
[46] M. Calligaris, O. Carugo. *Coord. Chem. Rev.*, **153**, 83 (1996).
[47] M. Calligaris. *Croat. Chem. Acta*, **72**, 147 (1999).
[48] N.S. Panina, M. Calligaris. *Inorg. Chim. Acta*, **334**, 165 (2002).
[49] (a) L. Canovese, M.L. Tobe, L. Cattalini. *J. Chem. Soc., Dalton Trans.*, 27 (1985); (b) P. Kapoor, K. Lovquist, A. Oskarsson. *J. Mol. Struct.*, **470**, 39 (1998); (c) S. Otto, L.I. Elding. *J. Chem. Soc., Dalton Trans.*, 2354 (2002); (d) J. Marques, T.M. Braga, F.A. Almeida Paz, T.M. Santos, M.F. Silva Lopes, S.S. Braga. *Biometals*, **22**, 541 (2009).
[50] R. Carter. *Molecular Symmetry and Group Theory*, p. 299, Wiley, New York, NY (1998).
[51] C.-K. Poon, C.-M. Che, *J. Chem. Soc., Dalton Trans*., 495 (1981).
[52] N.W. Alcock, J.C. Cannadine, G.R. Clark, A.F. Hill. *J. Chem. Soc., Dalton Trans*., 1131 (1993).
[53] A. Mercer, J. Trotter. *J. Chem. Soc, Dalton Trans*., 2480 (1975).
[54] For complex 5, the band is silent in infrared but has been detected in Raman spectrum.
[55] (a) G.A. Heath, A.J. Lindsay, T.A. Stephenson. *J. Chem. Soc., Dalton Trans*., 2429 (1982); (b) J.R. Barnes, R.J. Goodfellow. *J. Chem. Res. (M)*, 4301 (1979).
[56] K. Okamoto, C. Sasaki, Y. Yamada, T. Konno. *Bull. Chem. Soc. Jpn*, **72**, 1685 (1999).
[57] (a) G.E.D. Mullen, M.J. Went, S. Wocadlo, A.K. Powell, P.J. Blower. *Angew. Chem. Int. Ed. Engl.*, **36**, 1205 (1997); (b) G.E.D. Mullen, T.F. Fässler, M.J. Went, K. Howland, B. Stein, P.J. Blower. *J. Chem. Soc., Dalton Trans*., 3759 (1999).
[58] P. Maurer, A. Magistrato, U. Rothlisberger. *J. Phys. Chem. A*, **108**, 11494 (2004).
[59] J. Chatt, G.J. Leigh, A.P. Storace. *J. Chem. Soc. A*, 1380 (1971).
[60] (a) A.B.P. Lever, *Inorganic Electronic Spectroscopy*, 2nd Edn, p. 864, Elsevier, Amsterdam (1984); (b) E.I. Solomon, A.B.P. Lever, *Inorganic Electronic Structure and Spectroscopy*, *Methodology*, Vol. I, p. 732, Wiley, New York, NY (1999).
[61] V. Félix, T.M. Santos, J. Madureira, F. Mirante, S. Quintal, B.J. Goodfellow, M.G. Santana-Marques, J.P. de Jesus, M.G.B. Drew, M.J. Calhorda. *Inorg. Chim. Acta*, **356**, 335 (2003).
[62] (a) D.E. Janzen, D.G. Van Derveer, L.F. Mehne, D.A. Silva Filho, J.-L. Bredas, G.J. Grant. *Dalton Trans*., 1872 (2008); (b) D.E. Janzen, D.G. Van Derveer, L.F. Mehne, G.J. Grant. *Inorg. Chim. Acta*, 364, 1872 (2010); (c) C.A. Gamelas, N.A.G. Bandeira, C.C.L. Pereira, M.J. Calhorda, E. Herdtweck, M. Machuqueiro, C.C. Romão, L.F. Veiros. *Dalton Trans*., **40**, 10513 (2011); (d) E. Stephen, D.G. Huang, J.L. Shaw, A.J. Blake, D. Collison, E.S. Davies, R. Edge, J.A.K. Howard, E.J.L. McInnes, C. Wilson, J. Wolowska, J. McMaster, M. Schröder. *Chem. Eur. J*., **17**, 10246 (2011); (e) E. Stephen, A.J. Blake, E. Carter, D. Collison, E.S. Davies, R. Edge, W. Lewis, D.M. Murphy, C. Wilson, R.O. Gould, A.J. Holder, J. McMaster, M. Schröder. *Inorg. Chem.*, **51**, 1450 (2012).
[63] L.E. Roy, P.J. Hay, R.L. Martin. *J. Chem. Theory Comput.*, **4**, 1029 (2008).
[64] A.W. Ehlers, M. Bohme, S. Dapprich, A. Gobbi, A. Hollwarth, V. Jonas, K.F. Kohler, R. Stegmann, A. Veldkamp, G. Frenking. *Chem. Phys. Lett.*, **208**, 111 (1993).
[65] A detailed conformational study on ttbt and DFT calculations on complex 5 and other ttbt complexes of Ru (II) is underway and will be published separately. It focuses on the relevant local minima in PES, ttbt denticity clarification, which S atoms preferably bind, the crown thioether preferred geometrical arrangement and the relation between energy and the positioning of the monodentate ligands.
[66] M. Schmidt. In *High Performance Pigments*, E.B. Faulkner, R.J. Schwartz (Eds.), 2nd Edn, pp. 105–127, Wiley-VCH, Weinheim (2009).

[67] E. Alessio, G. Mestroni, G.A. Nardin, M. Wahib, M. Calligaris, G. Sava, S. Zorzet. *Inorg. Chem.*, **27**, 4099 (1988).
[68] T. Norrby, A. Börje, B. åkermark, L. Hammarström, J. Alsins, K. Lashgari, R. Norrestam, J. Mårtensson, G. Stenhagen. *Inorg. Chem.*, **36**, 5850 (1997).
[69] G. Wulfsberg, *Inorganic Chemistry*, p. 848, University Science Books, Sausalito, CA (2000).
[70] E. Zangrando, N. Kulisic, F. Ravalico, I. Bratsos, S. Jedner, M. Casanova, E. Alessio. *Inorg. Chim. Acta*, **362**, 820 (2009).
[71] S.R. Cooper. *Acc. Chem. Res.*, **21**, 141 (1988).
[72] M.J. Frisch, G.W. Trucks, H.B. Schlegel, *et al*. *Gaussian 03 (Revision D.02)*, Gaussian, Inc., Wallingford, CT (2004). See Supplementary Material for full citation.
[73] (a) P.J. Hay, W.R. Wadt. *Chem. Phys.*, **82**, 270 (1985); (b) W.R. Wadt, P.J. Hay. *Chem. Phys.*, **82**, 284 (1985); (c) P.J. Hay, W.R. Wadt. *Chem. Phys*., **82**, 299 (1985).
[74] M.P. Andersson, P. Uvdal. *J. Phys. Chem. A*, **109**, 2937 (2005).
[75] J.P. Merrick, D. Moran, L. Radom. *J. Phys. Chem. A*, **111**, 11683 (2007).
[76] G.A. Zhurko. Chemcraft v. 1.6. Available online at: http://www.chemcraftprog.com.
[77] R. Dennington, T. Keith, J. Millam. *GaussView (Version 5)*, Semichem Inc., Shawnee Mission, KS (2009).
[78] PyMOL Incentive Product, DeLano Scientific LLC (2006). The PyMOL Executable Build incorporates Open-Source PyMol 0.99rc6.
[79] S. Rawle, T.J. Sewell, S.R. Cooper. *Inorg. Chem.*, **26**, 376 (1987).